Cell Stem Cell, Volume *25*

Supplemental Information

Humanized Stem Cell Models of Pediatric Medulloblastoma Reveal an Oct4/mTOR Axis that Promotes Malignancy

Matko Čančer, Sonja Hutter, Karl O. Holmberg, Gabriela Rosén, Anders Sundström, Jignesh Tailor, Tobias Bergström, Alexandra Garancher, Magnus Essand, Robert J. Wechsler-Reya, Anna Falk, Holger Weishaupt, and Fredrik J. Swartling

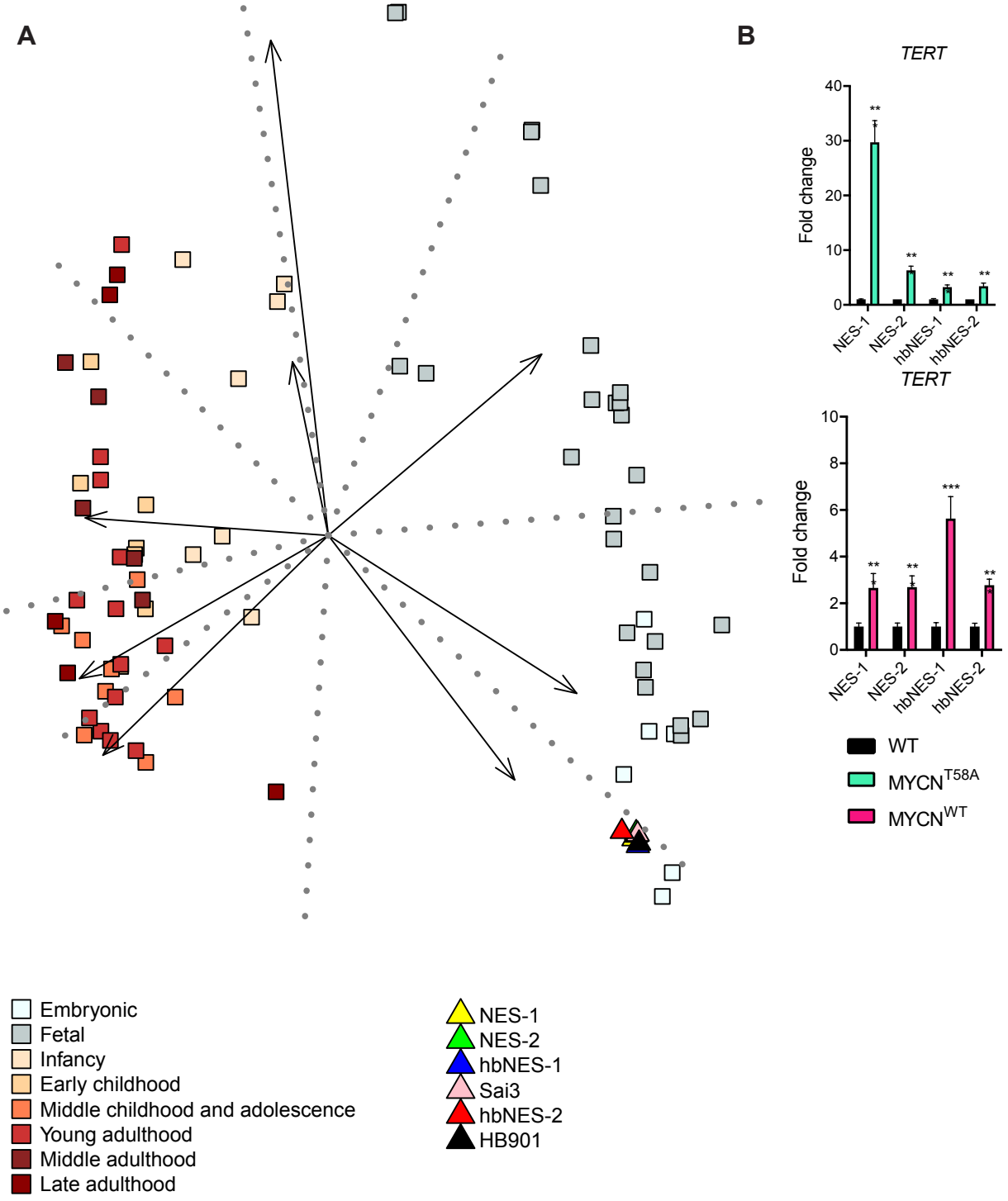

Figure S1. Classification of iPSC-derived and Human Neuro-Epithelial Stem (NES) Cells (Related to Figure 1)

(A) PCA plot of iPSC-derived and human NES cells with normal human brain samples (GSE25219) following metagene projection shows that these cells cluster with normal human embryonic samples.

(B) NES and hbNES pre-tumor cells upregulated *TERT* upon ectopic expression of $MYCN^{T58A}$ or $MYCN^{WT}$. *** indicate $p < 0.001$.

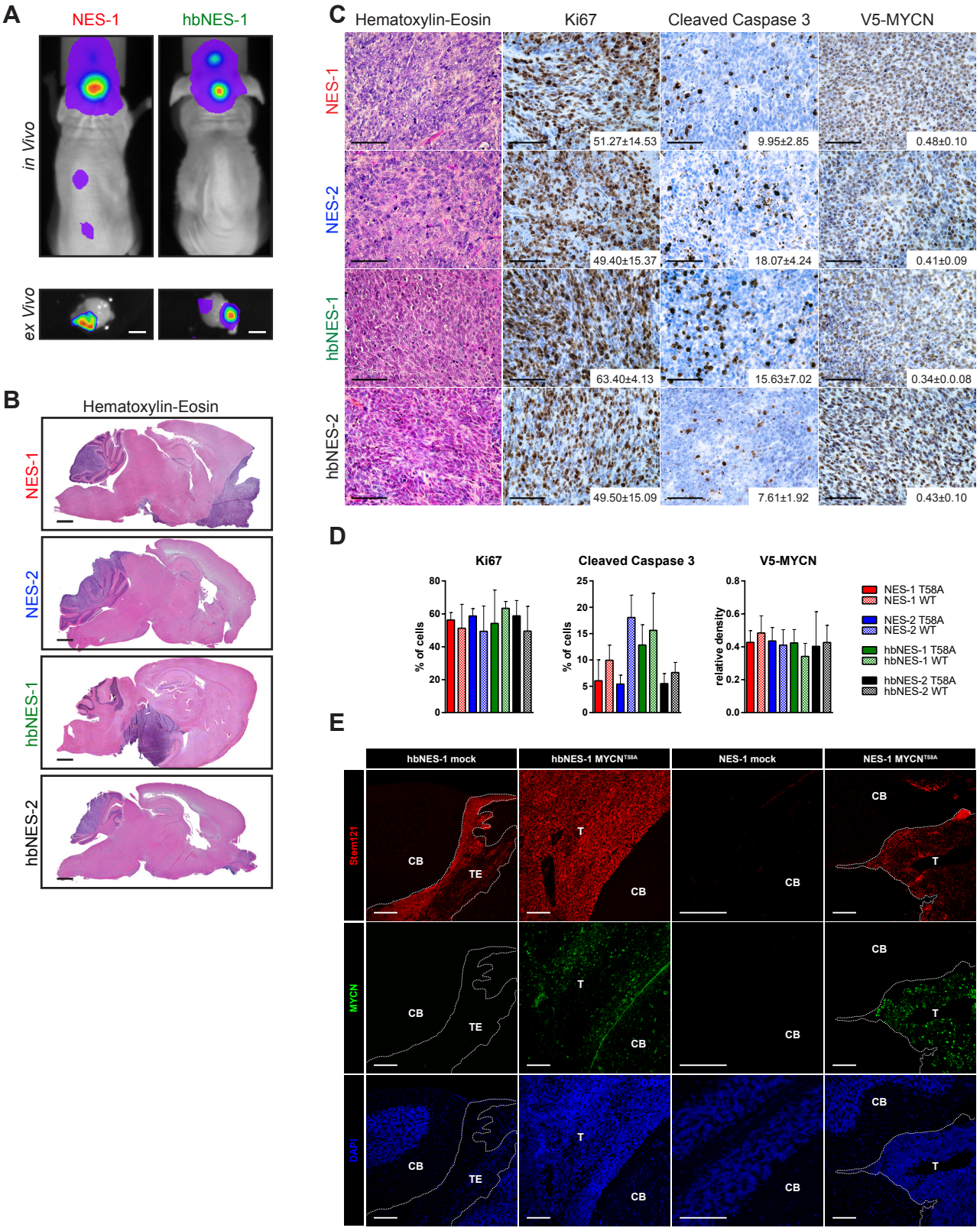

Figure S2. Histological Evaluation of NES and hbNES MYCN^{WT} tumors (Related to Figure 2)

(A) Representative bioluminescent images of mice bearing NES-1 and hbNES-1 MYCN^{T58A} tumors *in vivo* and *ex vivo*. Scale bars 5mm.

(B) Representative microphotographs of hematoxylin-eosin stained whole brains showing the location of NES-1, NES-2, hbNES-1 and hbNES-2 *MYCN^{T58A}* tumors. Microphotographs represent a panel of individual images that are stiched together as described in methods. Scale bars 1mm.

(C) Representative histological staining of NES and hbNES MYCN^{WT} tumors. Scale bars 50µm. Values indicate

% of positive cells (Ki67 and Cleaved Caspase 3) or relative density (V5-MYCN) measured from three individual tumors.
(D) Quantification of Ki67, Cleaved Caspase 3 and MYCN-V5 tag staining on 3 representative microphotographs of 3 tumors. Scale bars 50µm
(E) Immunofluorescent staining for human cell marker Stem121 and MYCN-V5 of cerebella transplanted with NES-1 mock, NES-1 $MYCN^{T58A}$, hbNES-1 mock and hbNES-1 $MYCN^{T58A}$ cells studied four weeks post cerebellar grafting. While *$MYCN^{T58A}$* expressing NES and hbNES cells developed into MYCN-V5-positive tumors, only hbNES-1 mock cells transiently proliferated to form MYCN-V5-negative neural tissue of human origin. Scale bars 100µm. CB=cerebellum, T=tumor, TE=stem cells

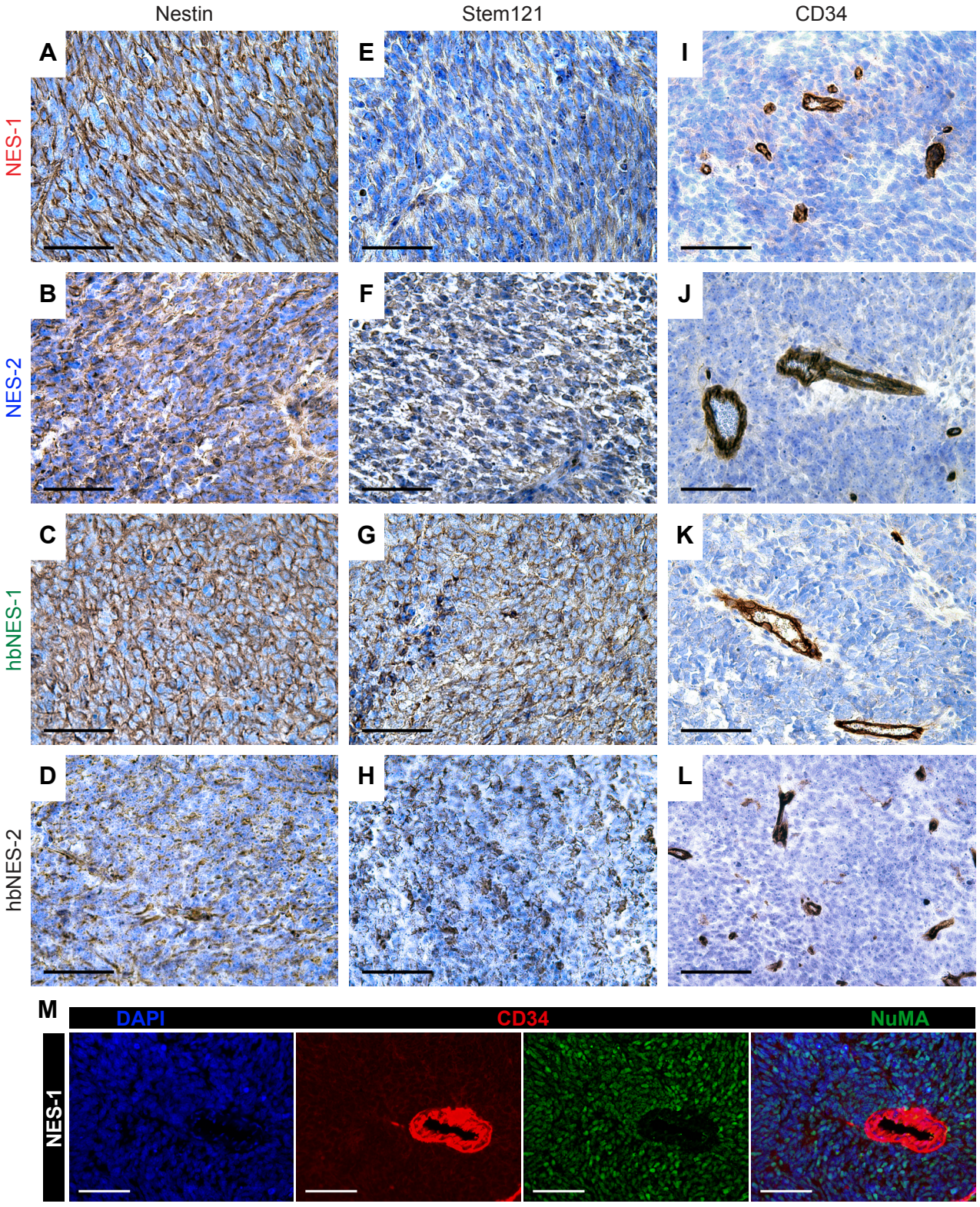

Figure S3. NES and hbNES MYCN^{T58A} Tumors Demonstrate Primitive Origin and Promote Angiogenesis (Related to Figure 3)

(A-D) Representative microphotographs of NES and hbNES tumors stained for primitive neuronal marker Nestin. Scale bars 50µm.

(E-H) Representative microphotographs of NES and hbNES tumors stained for human cell marker Stem121. Scale bars 50µm.

(I-L) Representative microphotographs of NES and hbNES tumors stained for vascular endothelial marker CD34. Scale bars 50µm.

(M) Immunofluorescence staining of CD34 and NuMA. Scale bars 50µm.

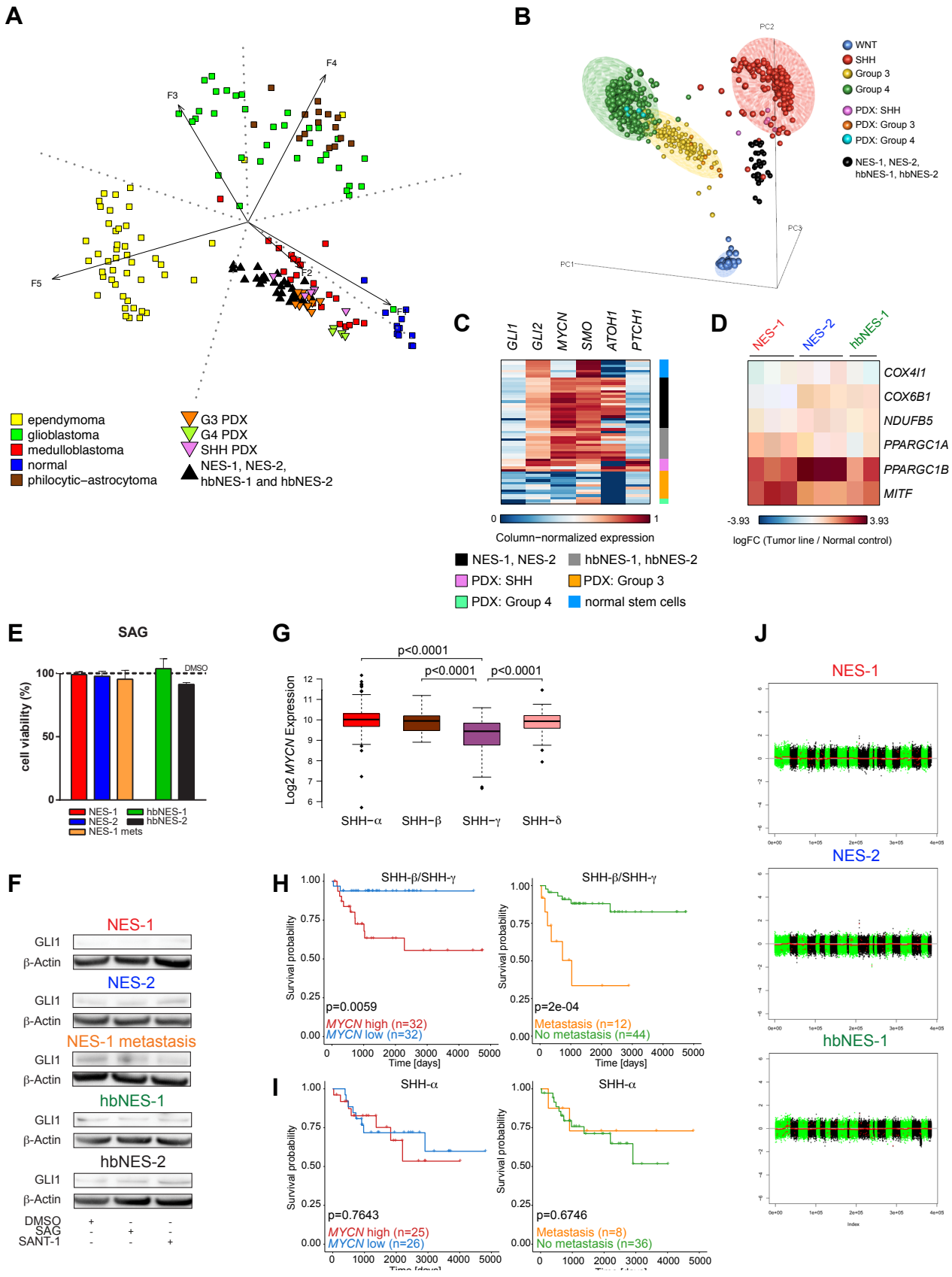

Figure S4. NES-1, NES-2 and hbNES Tumors Exhibit Expression Signature Specific for Medulloblastoma (Related to Figure 4)

(A) PCA plot following metagene projection of AmpliSeq gene expression data onto microarray gene expression for normal human brain samples (GSE25219) shows an alignment of NES-1, NES-2, hbNES-1 and hbNES-2 tumors, SHH-Xenografts, G3-Xenografts, and G4-Xenografts with MB patients.

(B) 3-dimensional PCA plot following metagene projection of AmpliSeq gene expression data onto microarray gene expression for human MB samples (GSE85217) in order to visualize MB subgroup affiliations.
(C) Heatmap illustrating gene-normalized expression of SHH MB markers *ATOH1*, *GLI1*, *GLI2*, *PTCH1*, *MYCN*, and *SMO* in stem cells, NES and hbNES tumors, and PDX models.
(D) Heatmap of log2 fold changes (logFC) of NES-1, NES-2, and hbNES-1 tumors compared to their respective stem cells showing generally higher expression of oxidative stress genes in the tumor models.
(E) SMO agonist SAG had no effect on viability of NES and hbNES tumor-derived cell lines. (F). SAG and SMO antagonist SANT-1 failed to change protein expression of SMO downstream target GLI1.
(G) Boxplot comparing the gene expression of *MYCN* between the SHH subsets (SHH-alpha, SHH-beta, SHH-gamma, SHH-delta; data from (Cavalli et al., 2017). The p-values reflect results of two-sided Welch's t-tests.
(H) Kaplan-Meier curves comparing overall survival between patients with high vs low expression of *MYCN* (left panel) or between patients with and without metastasis (right panel) within all SHH-β/-γ cases. The cut-off between high and low groups was chosen based on median expression and the p-value was obtained from the coxph score test (corresponding to log-rank test).
(I) Kaplan-Meier curves comparing overall survival between patients with high vs low expression of *MYCN* (left panel) or between patients with and without metastasis (right panel) within SHH-alpha cases. The cut-off between high and low groups was chosen based on median expression and the p-value was obtained from the coxph score test (corresponding to log-rank test).
(J) Representative plots illustrating log2 copy number ratios of NES-1, NES-2 and hbNES-1 tumors estimated from methylation data.

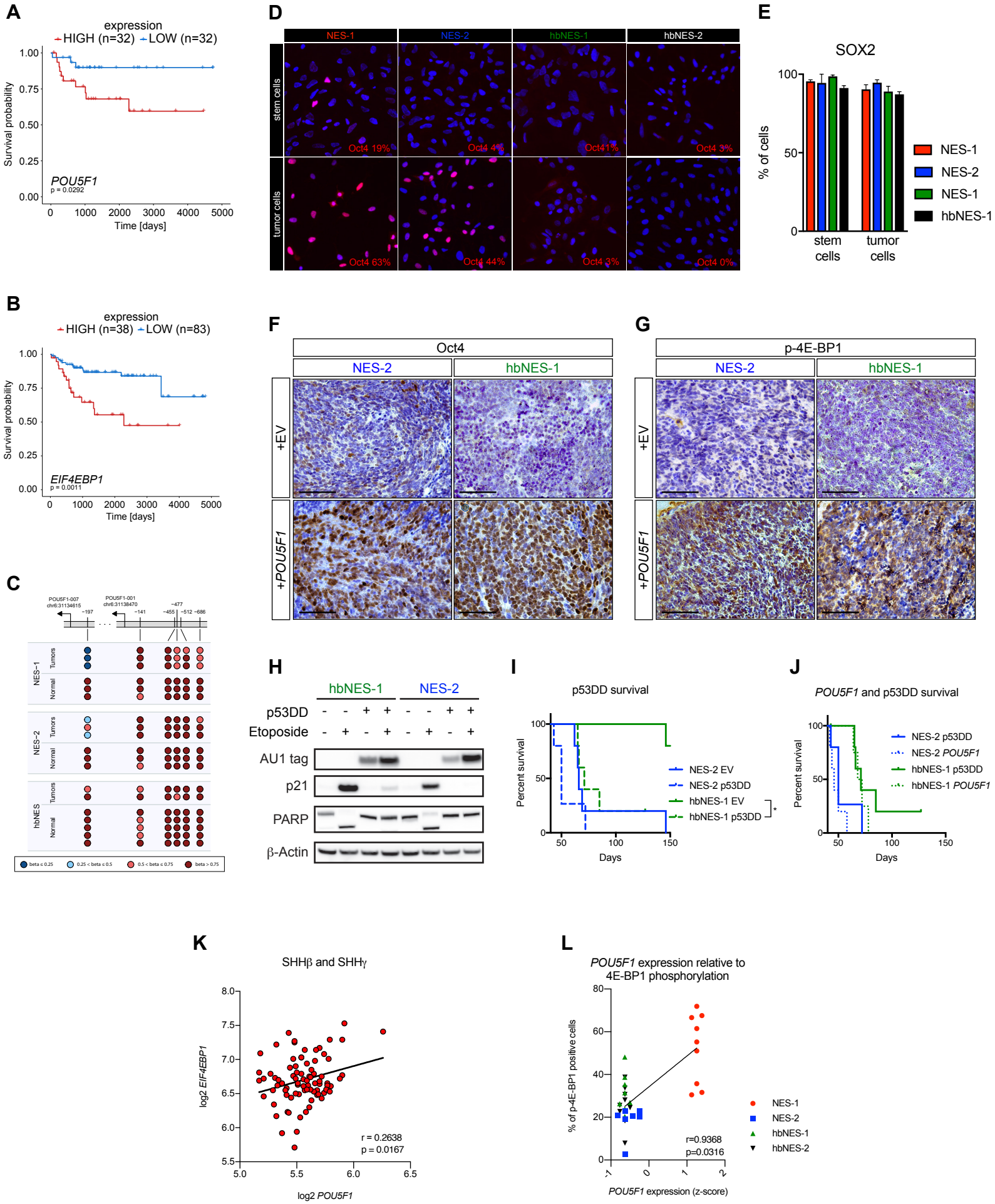
A
expression
HIGH (n=32)
LOW (n=32)
Survival probability
POU5F1
p = 0.0292
Time [days]
B
expression
HIGH (n=38)
LOW (n=83)
Survival probability
EIF4EBP1
p = 0.0011
Time [days]
C
POU5F1-007
chr6:31134615
POU5F1-001
chr6:31138470
NES-1
NES-2
hbNES
Tumors
Normal
beta ≤ 0.25
0.25 < beta ≤ 0.5
0.5 < beta ≤ 0.75
beta > 0.75
D
NES-1
NES-2
hbNES-1
hbNES-2
stem cells
tumor cells
Oct4 19%
Oct4 4%
Oct41%
Oct4 3%
Oct4 63%
Oct4 44%
Oct4 3%
Oct4 0%
E
SOX2
% of cells
stem cells
tumor cells
NES-1
NES-2
NES-1
hbNES-1
F
Oct4
NES-2
hbNES-1
+EV
+POU5F1
G
p-4E-BP1
NES-2
hbNES-1
+EV
+POU5F1
H
hbNES-1
NES-2
p53DD
Etoposide
AU1 tag
p21
PARP
β-Actin
I
p53DD survival
Percent survival
Days
NES-2 EV
NES-2 p53DD
hbNES-1 EV
hbNES-1 p53DD
J
POU5F1 and p53DD survival
Percent survival
Days
NES-2 p53DD
NES-2 POU5F1
hbNES-1 p53DD
hbNES-1 POU5F1
K
SHHβ and SHHγ
log2 EIF4EBP1
log2 POU5F1
r = 0.2638
p = 0.0167
L
POU5F1 expression relative to
4E-BP1 phosphorylation
% of p4E-BP1 positive cells
POU5F1 expression (z-score)
r=0.9368
p=0.0316
NES-1
NES-2
hbNES-1
hbNES-2

Figure S5. *POU5F1* and *EIF4EBP1* Correlate with the Poor Survival of SHH MB Patients and Aggressiveness of SHH MB Models (Related to Figure 5)

(A) Kaplan-Meier curve comparing overall survival between patients with high (n=32) vs low (n=32) expression of *POU5F1* demonstrates that high expression defines a high-risk group of patients within SHH infant (SHHβ and SHHγ) subtypes. Expression cut-off between high and low groups was selected based on median expression and the p-value was obtained from the coxph score test (corresponding to log-rank test).

(B) Kaplan-Meier curve comparing overall survival between patients with high (n=38) vs low (n=83) expression of *EIF4EBP1* in pediatric (<18 y) SHH patients. The expression cutoff was determined based on mean expression and the p-value was obtained from the coxph score test (corresponding to log-rank test).

(C) Comparison of *POU5F1* promoter methylation (showing probes up to 1000 bp upstream of the TSS) between NES-1, NES-2, and hbNES tumors and their respective stem cells. Methylation is shown as normalized beta-values for two transcripts (POU5F1-001 and POU5F1-007) which exhibited documented CCDS in the ENSEMBL database.

(D) Immunofluorescent Oct4 staining of stem cells of origin and respective tumor-derived cells. All hindbrain iPSC-derived and embryonal stem cells had, similar to RNA expression, very little to no Oct4 protein expression. While only iPSC-derived tumor cells NES-1 and NES-2 showed upregulation of Oct4, embryo-derived tumor cells hbNES-1 and hbNES-2 continued to express very low levels of Oct4 protein following malignant transformation.

(E) Quantification of SOX2 positive stem cells and tumor cells. Tumor cells retain high SOX2 levels throughout the malignant transformation with $MYCN^{T58A}$ and in vivo induction of tumors.

(F) Immunohistochemical analysis confirming high Oct4 protein levels in NES-2 *POU5F1* and hbNES-1 *POU5F1* tumors as compared to their EV counterparts. Scale bar 50μm.

(G) Immunohistochemical analysis of NES-2 and hbNES-1 tumor cells stably transduced with *POU5F1* expressing lentiviral vectors.

(H) Suppression of p53 function in hbNES-1 and NES-2 cells expressing the dominant-negative p53DD was confirmed by exposing respective cells to Etoposide (8h). Contrasting controls, cells expressing p53DD (AU1 tag) failed to upregulate p21 and showed almost no etoposide-induced apoptosis as demonstrated by PARP cleavage (lower band).

(I) Abrogation of the endogenous p53 function resulted in significant (*, $p < 0.05$) reduction in latency of hbNES-1 cells relative to empty-vector cells, while similar suppression in NES-2 cells demonstrated a strong trend in shorter latency ($p = 0.14$, Gehan-Breslow-Wilcoxon test)

(J) p53 activity suppression showed similar reduction in latency as *POU5F1* overexpression in both NES-2 ($p = 0.31$) and hbNES-1 ($p = 0.43$)

(K) *POU5F1* expression positively correlates with the expression of *EIF4EBP1* (4E-BP1) within SHHβ and SHHγ subtypes (Pearson correlation).

(L) Correlation comparison of *POU5F1* mRNA expression in NES and hbNES tumors in respect to the 4E-BP1 phosphorylation levels (Pearson correlation). *POU5F1* expression in NES and hbNES tumor tissue significantly correlates with the 4E-BP1 phosphorylation levels.

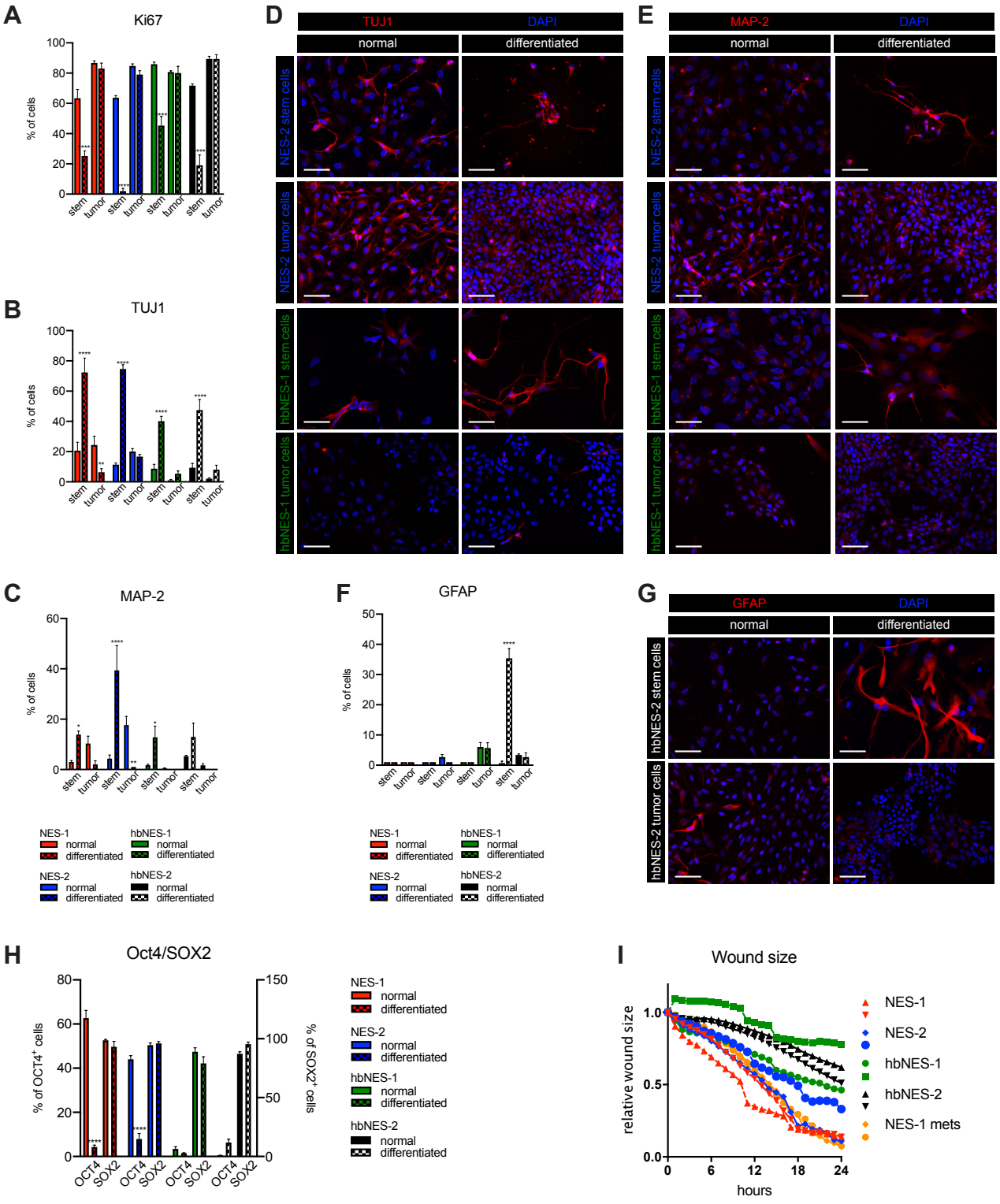

Figure S6. Immunofluorecence Staining of Non-Differentiated and Differentiated Primary and Tumor Cell Cultures. (Related to Figure 6)

(A) Quantification of the number of Ki67-positive proliferating cells in stem and tumor cell lines in normal, stem cell conditions and after 4 weeks of differentiation. While stem cells show a significant decrease in Ki67 following differentiation, tumor cells were not inhibited in proliferation.

(B-C) Differentiation of normal stem cells resulted in a significant increase in the number of cells positive for TUJ1 (B) and MAP-2 (C), while tumor cells remained only slightly positive for TUJ1 and MAP-2 after differentiation.

(D-E) Immunofluorescent staining against TUJ1 (D) and MAP-2 (E) of representative stem and tumor cells

before and after differentiation.
(F) Quantification of GFAP staining of stem and tumor cell lines in normal, stem cell conditions and after differentiation. Only hbNES-2 stem cells significantly elevated astrocytic marker GFAP following the differentiation.
(G) Representative microphotographs of GFAP immunostaining of hbNES-2 stem and tumor cells before and after differentiation.
(H) Following the differentiation all NES tumor cells significantly reduced Oct4 levels, while in both NES and hbNES tumor cells SOX2 levels remained unchanged.
(I) Relative wound size of a scratch migration assay plotted against time showing a complete wound closure in NES cells and NES-1 metastases, while hbNES cells did not completely close the wound after 24h.
*, ** and **** indicate $p<0.05$, $p<0.01$ and $p<0.0001$, respectively. Scale bar=50μm.

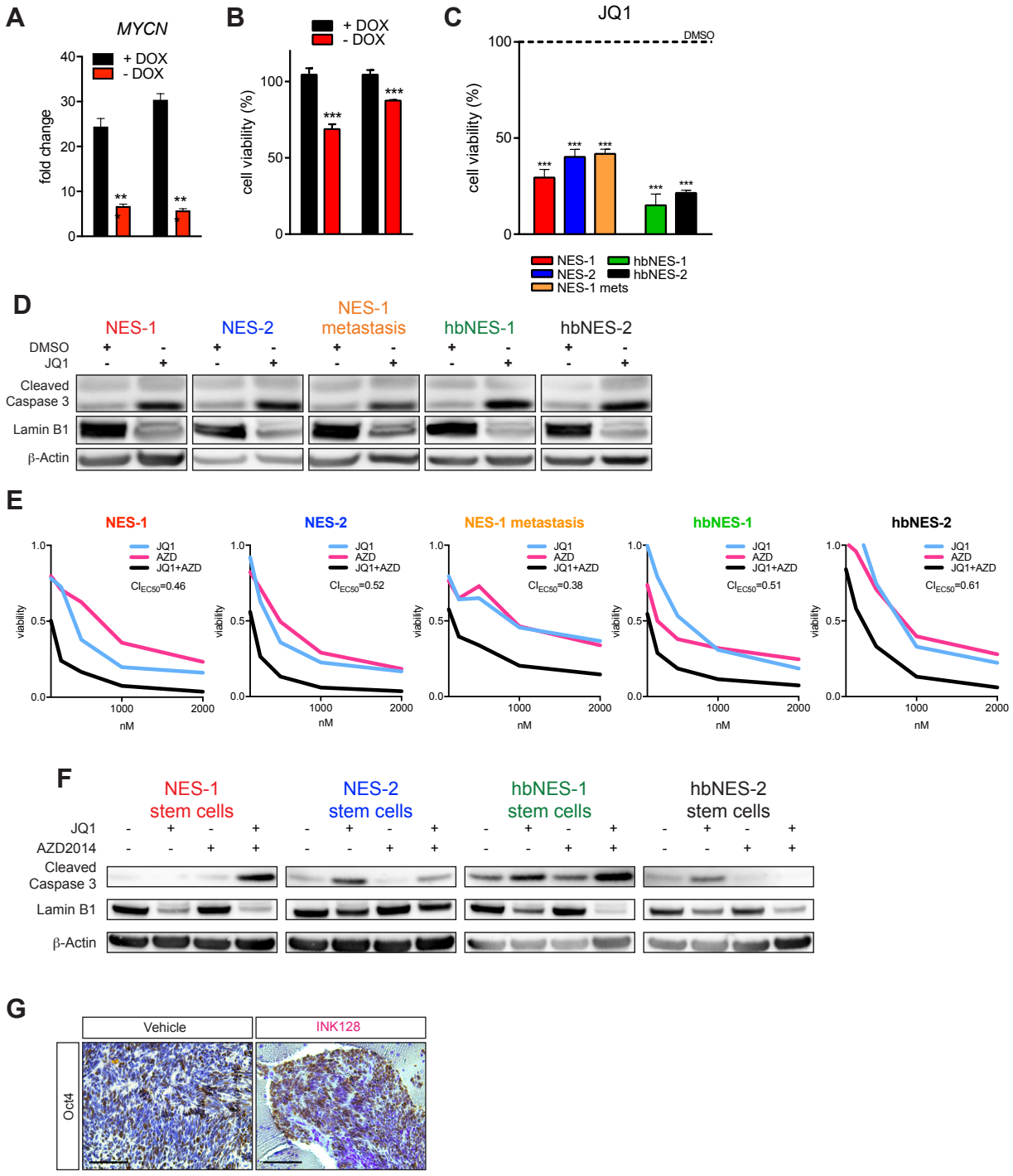

Figure S7. Genetic and Pharmacological Suppression of *MYCN* Signaling Induces Apoptosis and Senescence in NES and hbNES Cell Cultures (Related to Figure 7)

(A) Conditional *MYCN* knock-down significantly represses *MYCN* RNA in NES-1-derived tumor cultures.

(B) *MYCN* repression by Doxycycline (DOX) removal leads to significant decrease in cell viability of NES-1-derived tumor cultures after 6 days.

(C) JQ1 significantly decreases viability of NES- and hbNES-derived tumor cultures and suppresses viability of cells derived from NES-1 spinal cord metastases.

(D) JQ1 treatment induced apoptosis and senescence as seen by increase in Cleaved Caspase 3 and decrease in Lamin B1 after 72h in NES, hbNES and cells derived from NES-1 spinal cord metastases.

(E) BET and mTOR inhibitors synergize to reduce viability of NES and hbNES tumor cultures. CI scores were computed as described in Methods and CI score < 0.80 was considered synergistic.

(F) Combined BET and mTOR inhibition induced cellular senescence in embryonic and iPSC-derived neuroepithelial stem cells.
(G) Representative Oct4 staining microphotographs of NES-1 tumors treated for 8 days with 1mg/kg INK128 or vehicle. Scale bar=50μm.
*** $p < 0.001$.

Supplementary Tables

Table S1. Tumor models and tumor-derived cell lines.

Name	Parental Cell Line	Tumor Type	Transgene	Passages *In Vitro*
A3-24	Sai2	hbNES-1	*MYCN*^{T58A}	5+
A3-33	Sai2	hbNES-1	*MYCN*^{T58A}	12+
A3-41	AF22	NES-1	*MYCN*^{T58A}	16+
A3-43	AF22	NES-1	*MYCN*^{T58A}	19+
A4-4M[§]	A3-41	Metastasis	*MYCN*^{T58A}	12+
A4-20M[§]	A3-45	Metastasis	*MYCN*^{T58A}	13+
A6-13	CTRL-3-NES	NES-2	*MYCN*^{T58A}	14+
A6-20	CTRL-3-NES	NES-2	*MYCN*^{T58A}	13+
A7-14	HB930	hbNES-2	*MYCN*^{T58A}	15+
A7-20	HB930	hbNES-2	*MYCN*^{T58A}	15+

[§]cell line derived from spinal cord metastasis

Related to Figure 2 and STAR Methods.